Volume 3 | Number 26 | 14 July 2015 | Pages 5125–5378

Journal of Materials Chemistry B

Materials for biology and medicine

www.rsc.org/MaterialsB

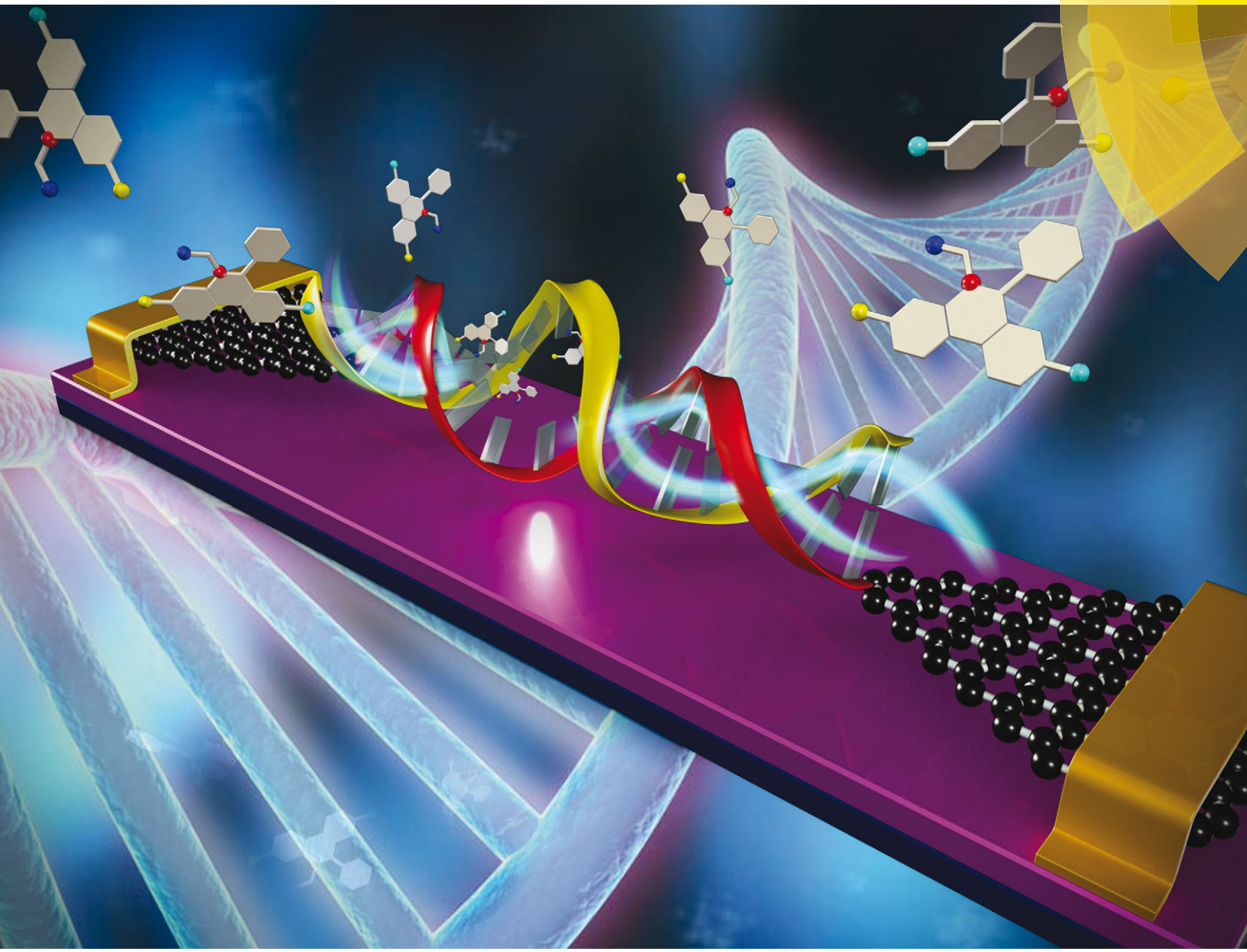

ISSN 2050-750X

ROYAL SOCIETY OF CHEMISTRY

COMMUNICATION

Xuefeng Guo *et al.*

Revealing the direct effect of individual intercalations on DNA conductance toward single-molecule electrical biodetection

Journal of
Materials Chemistry B

COMMUNICATION

View Article Online
View Journal | View Issue

Cite this: J. Mater. Chem. B, 2015, 3, 5150

Received 11th April 2015,
Accepted 22nd May 2015

DOI: 10.1039/c5tb00666j

www.rsc.org/MaterialsB

Revealing the direct effect of individual intercalations on DNA conductance toward single-molecule electrical biodetection†

Xiaolong Wang,‡[a] Li Gao,‡[a] Bo Liang,[b] Xin Li[b] and Xuefeng Guo*[ac]

Monitoring complex interactions of biological systems at the molecular level provides new opportunities to uncover fundamental details of the basic processes of life, of crucial importance to biology, diagnosis and drug discovery. Here, we detailed a reliable single-molecule electrical approach for achieving label-free, ultrasensitive electrical detection of DNA functions, using DNA intercalations by individual EB/SGs as a representative, based on DNA-functionalized molecular junctions. The analysis principle relies on the distortion mechanism of intercalative binding on the structural integrity of DNAs at the single-event level, resulting in significant step-wise changes in DNA charge transport. Such an understanding led to direct, rapid intercalator detection with subfemtomolar sensitivity. This single-molecule electrical approach provides a foundation for future molecular dynamics studies with single-molecule sensitivity, which will lead to direct observation of new effects and fundamental discoveries of the details of the most basic processes of life.

Monitoring complex interactions between biomolecules at the molecular level, such as intercalative DNA binding that is ubiquitous in biological systems, is fundamentally important for a wide variety of biological functions (such as DNA synthesis and gene expression), which holds great potential for applications in different areas ranging from DNA visualization and gene mutation detection to disease diagnosis and drug discovery.[1–4] Therefore, many reports have investigated the intercalative effects of planar polycyclic aromatic organic intercalators, such as ethidium, acridine, metal complexes and their derivatives, on the physicochemical properties of DNAs.[1–7] In this study, we described a unique method for directly probing how these individual intercalative interactions affect the electrical properties of DNAs based on DNA-functionalized molecular junctions, using two widely used intercalators (ethidium bromide (EB) and SYBR Green I (SG)) as representatives (Fig. 1). The feature of particular interest used here is that these fundamental intercalation processes, through either classical intercalation or groove binding,[5–7] lead to profound changes in the structural integrity of DNAs, such as stabilization, lengthening, stiffening, and unwinding of the double helix.[8,9] The degree of DNA bending varies depending on the intercalators.[10–13] For example, the intercalation of EB both increases the distance between base pairs by approximately 0.3 nm and unwinds the double helix by 26°.[14–16] To explore how these intercalation-induced local distortions and/or unwinding of the DNA structures change the charge transport properties of DNAs,[17–19] single DNA duplexes were integrated into electrical nanocircuits. These nanocircuit-based architectures displayed the capability of achieving direct, label-free, rapid electrical detection of intercalating interactions at the

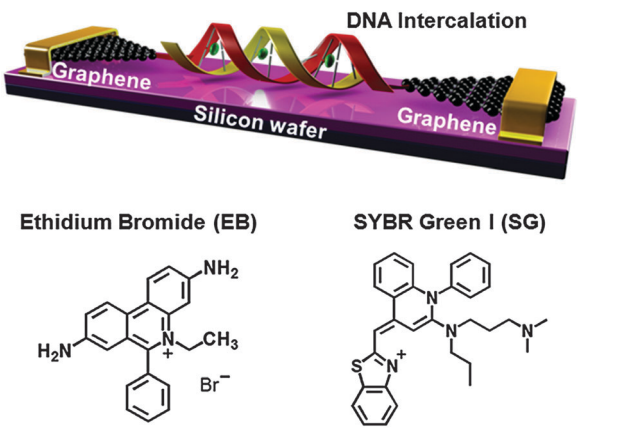

Fig. 1 Schematic representation of DNA-functionalized molecular junctions used for examining the effect of EB or SG intercalations on DNA charge transport, and the molecular structures of EB[6] and SG.[28]

[a] Center for Nanochemistry, Beijing National Laboratory for Molecular Sciences, State Key Laboratory for Structural Chemistry of Unstable and Stable Species, College of Chemistry and Molecular Engineering, Peking University, Beijing 100871, P. R. China. E-mail: guoxf@pku.edu.cn
[b] Adesso Advanced Materials Wuxi Co., Ltd, Huihong Industrial Park, 18 Xishi Road, New District, Wuxi, Jiangsu Province, 214000, P. R. China
[c] Department of Materials Science and Engineering, College of Engineering, Peking University, Beijing 100871, P. R. China

† Electronic supplementary information (ESI) available: Materials, detailed device fabrication, and control experiments. See DOI: 10.1039/c5tb00666j

‡ These authors contributed equally.

single-event level, thus providing a reliable single-molecule electrical approach that is able to interface electronic circuits with biological systems by using DNAs as conductive biocompatible bridges. These findings also created fast, label-free, and low-cost tools for detecting trace amounts of target analytes. In fact, the utility of the intercalation-induced distortion of the DNA structures is an important method to produce novel activities and build new types of optical or electrochemical DNA-based biosensors.[20–27]

To date, several approaches based on nanomaterials and nanostructures have been successfully developed for ultrasensitive electrical biosensor fabrication, including carbon nanomaterials,[29–38] silicon nanowires,[39–42] nanopores/nanoclusters,[43,44] molecular junctions,[45–49] and others.[50,51] Recently, we and our coworkers developed two lithographic methods to covalently wire one or a few molecules onto both facing ends of nanogaps ($\leq$10 nm), in either single-walled carbon nanotubes (SWNTs) or graphene, to build stable molecular electronic devices.[52,53] An important feature of these techniques is the ability to build robust molecule–electrode linkages by covalent amide bond formation, which can tolerate a wide range of chemical treatments. In conjunction with the electrical properties of carbon-based electrodes and the ease of device fabrication, the stability of the devices promotes carbon electrode-based molecular junctions as reliable testbeds for molecular electronics.[54–56] This provides the foundation for monitoring biomolecular interactions at the single-event level.

In the following study, DNA-functionalized molecular junctions were formed from indented graphene point contact arrays generated by a dash-line lithographic (DLL) method.[53] The fabrication details can be found in the ESI.† Under optimized conditions, the maximum connection yield for DNA molecules was approximately 27%, which corresponded to the cutting yield of approximately 36%.[57] On the basis of these data, the analysis of the number of junctions that contribute to charge transport, using the binomial distribution, demonstrated that in most cases, only one or two junctions contribute to the charge transport of the devices.[53]

Fig. 2a shows the comparison of the current–voltage (I–V) curves of a representative DNA-reconnected device before and after cutting (forming a nanogap by electron beam lithography and oxygen plasma etching), respectively. In brief, the black curve shows the source–drain current (I_D) plotted against the gate voltage (V_G) at constant source–drain bias voltage (V_D = −50 mV) before cutting. We note that all the graphene devices before cutting exhibit p-type electric field effects with little gate dependence because the neutrality point (I_{NP}) of graphene shifted to the more positive value, which is probably due to chemical doping and/or charge transfer induced by etching agents and polymer resists used (iron nitrate and PMMA). The red curve, obtained after cutting, shows no conductance down to the noise limit of the measurement ($\leq$100 fA) because of the nanogaps. To eliminate possible artifacts from gate hysteresis, all the I–V curves were carefully acquired on the same measurement cycle, while scanning from positive to negative biases. We observed very stable I–V curves for these devices under fixed experimental conditions and then they were used to detect DNA

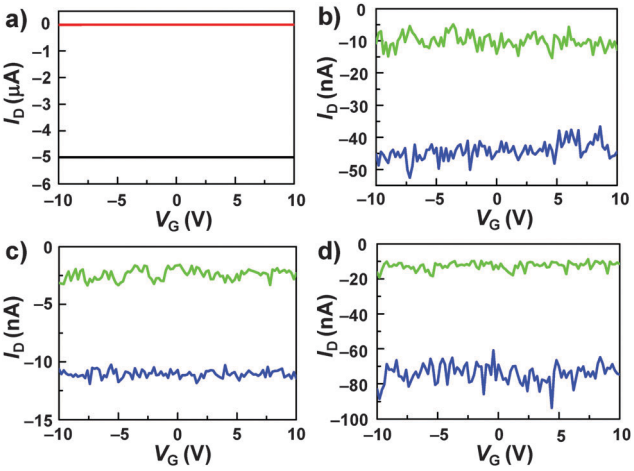

Fig. 2 (a) Device characteristics of a representative DNA-rejoined junction before (black) and after (red) cutting. The structure of the DNA used can be found in the ESI.† (b–d) Device characteristics of different DNA-rejoined devices after DNA connection (blue) and after further EB treatments (green) at different concentrations (b: 5.0×10^{-7} mol L^{-1}; c: 5.0×10^{-10} mol L^{-1}; d: 5.0×10^{-13} mol L^{-1}) for 30 minutes. All measurements were performed at V_D = −50 mV.

connection and for sensing functions. Treatments of either DNAs or intercalators change the conductance of pristine graphene because of nonspecific adsorption of molecules on the surface of graphene through π–π interaction (Fig. S1a, ESI†). Therefore, Triton X-100 (1%, V/V), a nonionic surfactant, was used to treat the graphene surface. This treatment is important because Triton X-100 can be adsorbed onto graphene surfaces as a blocking layer to prevent nonspecific binding of both DNAs and intercalators on graphene, as demonstrated in Fig. S1b (ESI†). It is also known that the ionic strengths and concentrations of the solution in which the measurement is carried out may influence the device current. Therefore, we carefully performed the measurements under the same conditions as described in the ESI.† These efforts rule out potential artifacts originating from the effects of nonspecific adsorption or ions on the device conductance, which is consistent with previous studies on polymer coating for selective biofunctionalization.[58,59] After the completely cut devices were treated with Triton X-100, we used them for DNA connection. After DNA connection, we observed the recovery of the device conductance, albeit at reduced current values (blue trace in Fig. 2b). These observations were consistent with our previous reports.[52,53]

After further EB treatment (1×10^{-7} mol L^{-1}) for 30 minutes, we observed an obvious decrease in device conductance (green trace in Fig. 2b). This observation could be explained by the fact that EB intercalation results in the distortion of the π-stacking integrity of the double helical structure, as shown by previous reports.[15,16] This distortion of the structural integrity of DNA duplexes varies the DNA charge transport, consistent with previous studies that demonstrated the sensitivity of DNA conductivity to protein binding.[17] To rule out other potential artifacts originating from Schottky barrier modification and/or

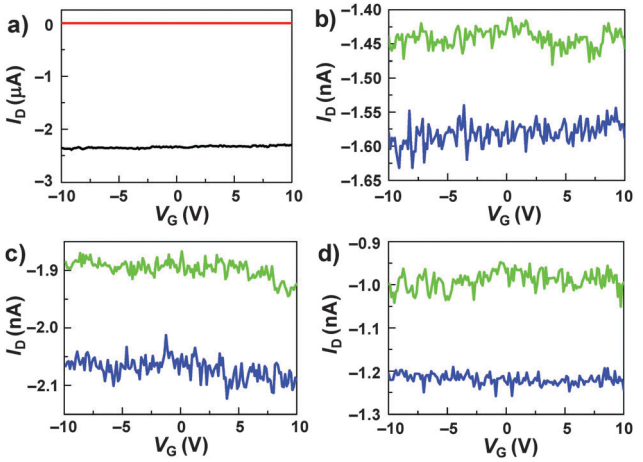

Fig. 3 (a, b) Comparisons of the electrical characteristics of the same device before cutting (black), after cutting (red), after DNA connection (blue) and after further SG treatments (green) (2.0×10^{-12} mol L^{-1}). (c, d) *I–V* curves of another two working devices after DNA connection (blue) and after further SG treatments (green) at different concentrations (c: 2.0×10^{-13} mol L^{-1}; d: 2.0×10^{-14} mol L^{-1}). The time for SG treatments is about 30 minutes. All measurements were performed at V_D = −50 mV.

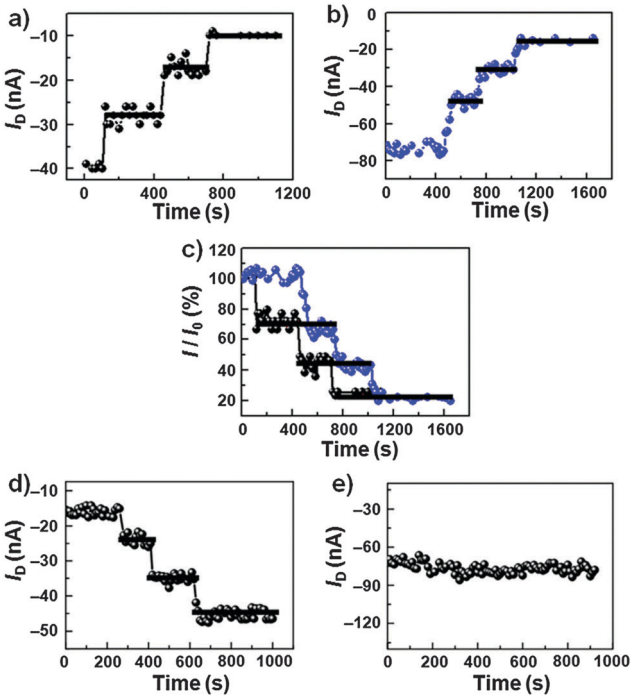

Fig. 4 (a, b) Changes in I_D as a function of time at different EB concentrations (a: 5.0×10^{-7} mol L^{-1}; b: 5.0×10^{-13} mol L^{-1}). (c) Comparisons of the corresponding I_D change ratios (black: 5.0×10^{-7} mol L^{-1}; blue: 5.0×10^{-13} mol L^{-1}). (d) EB degradation process of the same device used in (b) when exposed to light after EB treatment. The light intensity was approximately 12.8 mW cm^{-2}. (e) Control experiment using the same device before EB treatment, showing no obvious I_D changes under the same irradiation conditions. All the measurements were performed at V_D = −50 mV and V_G = 0 V.

nonspecific surface adsorption, we performed control experiments using partially cut graphene devices where the graphene was not fully cut during oxygen-plasma etching. We found that none of the devices showed detectable variations in conductance under the same operating conditions (Fig. S2, ESI†). This is reasonable because both the graphene surface and the contact interface between gold and graphene have been protected by Triton X-100. In addition, control experiments monitoring the conductance of DNA-rejoined devices in an ambient environment and after water treatments (Fig. S3, ESI†) did not show obvious current changes, thus excluding possible effects of either the detection environment or water. To prove the universality of this observation, we also tested another intercalator, SG, to carry out the same experiments. We observed similar results to those gained using EB, as shown in Fig. 3a and b.

To test the sensitivity of these graphene–DNA junctions, we investigated their electrical behaviors by simply altering the intercalator concentrations. Different DNA-rejoined devices were used for each EB or SG concentration. Fig. 2c, d and 3c, d, show representative *I–V* curves in each case, before and after EB or SG treatments. Consistently, all the working devices (at least 20 devices) displayed conductance decreases to different extents, although there were variations in conductance from device to device, thus demonstrating good detection reliability and reproducibility. The highest sensitivities achieved were at approximately 5.0×10^{-13} mol L^{-1} for EB and approximately 2.0×10^{-14} mol L^{-1} for SG. Remarkably, these detection limits are significantly lower than those of previously reported DNA sensors, such as 2.0×10^{-10} mol L^{-1} (EB),[60] 5.0×10^{-9} mol L^{-1} (EB),[61] and 6.0×10^{-8} mol L^{-1} (SG).[28] In principle, our devices could be employed to sense intercalative DNA binding at the single-molecule level because they have only one or at most two DNA duplexes for intercalation, as demonstrated below.

The dynamic process of DNA intercalation was carefully studied by real-time monitoring of the interacting processes between DNAs and targets of interest by electrical signals through a simple dipping method. Fig. 4a and b show the time traces of the intercalation processes at different EB concentrations. Fig. 4c shows the corresponding changes in current ratios (I/I_0, I_0 is the original I_D) as a function of time. We found that the collective diffusion and binding of EB molecules were concentration-dependent while the intercalation rate of individual EBs is similar, completed within 30 seconds. The former time-dependent behavior is reasonable, because the rate of the binding reaction between individual DNAs and EB molecules is proportional to the EB concentration, although the actual diffusion rate of individual EBs does not change at different EB concentrations. If the concentration of EB is lower, the reaction rate is generally slower, resulting in a longer reaction time. More interestingly, the binding process at each concentration displayed consistent step-wise current decreases. Although the concentrations had a six-order-magnitude difference, they showed surprising dynamic procedures, with the same number of "steps" and similar values of the corresponding current ratios (approximately 70%, 40% and 20% for the different steps, respectively). After EB treatments for a sufficient time (30 minutes), the ultimate current ratio was approximately

20%, which was consistent with the results shown in Fig. 2. This observation can be explained by the fact that our device consists of only one or at most two DNA molecules spanning the nanogaps. The feature of three steps suggests that the double-stranded DNAs of about 20 base pairs used here could adopt three individual EB molecules, which is consistent with the results reported previously.[8,9] This sensing property without concentration dependence proved that these devices could be used to monitor EB intercalations at the single-event level. Similar results were reported recently in a study based on an optical method.[62] Unlike EB intercalation, SG intercalation did not produce consistent results (the final current ratio) at various concentrations (Fig. 3). This difference between the effects of EB and SG intercalations on DNA charge transport stems from their specific intercalating modes: classical insertion for EB[6] and groove binding for SG.[28] The former can break the π-stacking integrity of DNA base pairs that form the conducting channel, while the latter only induces the interaction of intercalators with DNA major and/or minor grooves, which has weaker and uncertain influences on the charge-transporting properties of DNAs.[6]

Finally, to further prove the above-observed effect of EB intercalation on DNA conductivity, the time-dependent process of EB degradation upon exposure to light was explored. After fresh DNA-rejoined devices were treated with EB molecules for 30 minutes, they were exposed to light with an intensity of approximately 12.8 mW cm^{-2}. Fig. 4d shows the conductance recovery dynamics of the same device used in Fig. 4b. With the increase in exposure time, the DNA conductance converted back to nearly 70% of its original value in a step-wise manner (response time, approximately 30 seconds), which is exactly opposite to the EB intercalation demonstrated above. This is because light induces the gradual decomposition of individual EBs, thus leading to the step-by-step recovery of the initial conformation (and thus the initial conductance) of DNAs. The presence of EB residues after degradation hampers the full recovery of the initial conformation of DNAs; therefore, the DNA conductance could not completely recover the initial value. Control experiments using the same device before EB treatment did not show obvious current changes under the same irradiation conditions (Fig. 4e). Again, this strongly proves the important role of EB intercalation in the electrical properties of DNAs.

In summary, we described a reliable single-molecule electrical biosensor for directly revealing the intrinsic effect of individual EB/SG intercalations on DNA charge transport based on DNA-functionalized molecular junctions. The analysis principle relies on the distortion mechanism of intercalative binding on the structural integrity of DNAs at the single-event level, resulting in significant step-wise changes in DNA conductance. Such an understanding offered direct, rapid intercalator detection with subfemtomolar sensitivity. Compared with traditional optical methods, this nanocircuit-based architecture is complementary, but with obvious advantages such as avoiding problems with bleaching and fluorescence labelling. Therefore, this single-molecule electrical approach provides a foundation for future molecular dynamics studies with single-molecule sensitivity, which will lead to direct observation of new effects and fundamental discoveries of the details of the most basic processes of life. We expect that this approach will stimulate research in a wide variety of fields, for example fundamental biology, clinical diagnostics, health improvement, drug discovery, and bioterrorism prevention.

Acknowledgements

We acknowledge primary financial support from MOST (2012CB921404) and NSFC (21225311, 91333102, and 21373014).

Notes and references

1 R. Martinez and L. S. Chacon-Garcia, *Curr. Med. Chem.*, 2005, **12**, 127.
2 J. Liu, Z. Cao and Y. Lu, *Chem. Rev.*, 2009, **109**, 1948.
3 X. Xie, W. Xu and X. Liu, *Acc. Chem. Res.*, 2012, **45**, 1511.
4 Y. Takezawa and M. Shionoya, *Acc. Chem. Res.*, 2012, **45**, 2066.
5 M. J. Waring, *Annu. Rev. Biochem.*, 1981, **50**, 159.
6 H. Liu and P. J. Sadler, *Acc. Chem. Res.*, 2011, **44**, 349.
7 in *Molecular Aspects of Anticancer Drug Action*, ed. S. Neidle and M. J. Warring, MacMillian, London, 1983.
8 H. Ihmels and L. Thomas, in *In Materials Science of DNA*, ed. J. I. Jin and J. Grote, Taylor and Francis Group, US, 2012, pp. 49–75.
9 A. Celedon, D. Wirtz and S. Sun, *J. Phys. Chem. B*, 2010, **114**, 16929.
10 P. Cluzel, A. Lebrun, C. Heller, R. Lavery, J. L. Viovy, D. Chatenay and F. Caron, *Science*, 1992, **258**, 1122.
11 I. D. Vladescu, M. J. McCauley, M. E. Nuñez, I. Rouzina and M. C. Williams, *Nat. Methods*, 2007, **4**, 517.
12 M. S. Rocha, M. C. Ferreira and O. N. Mesquita, *J. Chem. Phys.*, 2007, **127**, 105108.
13 I. D. Vladescu, M. J. McCauley, I. Rouzina and M. C. Williams, *Phys. Rev. Lett.*, 2005, **95**, 158102.
14 H. M. Sobell, C. Tsai, S. C. Jain and S. G. Gilbert, *J. Mol. Biol.*, 1977, **114**, 333.
15 H. M. Berman and P. R. Young, *Annu. Rev. Biophys. Bioeng.*, 1981, **10**, 87.
16 C. C. Tsai, S. C. Jain and H. M. Sobell, *J. Mol. Biol.*, 1977, **114**, 333.
17 J. C. Genereux and J. K. Barton, *Chem. Rev.*, 2010, **110**, 1642.
18 T. Takada, M. Fujitsuka and T. Majima, *Proc. Natl. Acad. Sci. U. S. A.*, 2007, **104**, 11179.
19 S. P. Liu, S. H. Weisbrod, Z. Tang, A. Marx, E. Scheer and A. Erbe, *Angew. Chem., Int. Ed.*, 2010, **49**, 3313.
20 E. D. Horowitz, A. E. Engelhart, M. C. Chen, K. A. Quarles, M. W. Smith, D. G. Lynn and N. V. Hud, *Proc. Natl. Acad. Sci. U. S. A.*, 2010, **107**, 5288.
21 T. D. Tullius and S. J. Lippard, *Proc. Natl. Acad. Sci. U. S. A.*, 1982, **79**, 3489.
22 L. Kong, J. Xu, Y. Xu, Y. Xiang, R. Yuan and Y. Q. Chai, *Biosens. Bioelectron.*, 2013, **42**, 193.

23 J. D. Slinker, N. B. Muren, S. E. Renfrew and J. K. Barton, *Nat. Chem.*, 2011, **3**, 228.
24 Z. Zhang, X. Wang, Y. Wang and X. Yang, *Analyst*, 2010, **135**, 2960.
25 A. I. Dragan, E. S. Bishop, R. J. Strouse, J. R. Casas-Finet, M. A. Schenerman and C. D. Geddes, *Chem. Phys. Lett.*, 2009, **480**, 296.
26 J. Wang, *Anal. Chim. Acta*, 2002, **469**, 63.
27 P. A. Sontz, N. B. Muren and J. K. Barton, *Acc. Chem. Res.*, 2012, **45**, 1792.
28 H. Zipper, H. Brunner, J. Bernhagen and F. Vitzthum, *Nucleic Acids Res.*, 2004, **32**, e103.
29 W. Yang, K. R. Ratinac, S. P. Ringer, P. Thordarson, J. J. Gooding and F. Braet, *Angew. Chem., Int. Ed.*, 2010, **49**, 2114.
30 B. L. Allen, P. D. Kichambare and A. Star, *Adv. Mater.*, 2007, **19**, 1439.
31 T. Cohen-Karni, Q. Qing, Q. Li, Y. Fang and C. M. Lieber, *Nano Lett.*, 2010, **10**, 1098.
32 Q. Y. He, H. G. Sudibya, Z. Y. Yin, S. X. Wu, H. Li, F. Boey, W. Huang, P. Chen and H. Zhang, *ACS Nano*, 2010, **4**, 3201.
33 S. Liu and X. F. Guo, *NPG Asia Mater.*, 2012, **4**, e23.
34 Y. K. Choi, I. S. Moody, P. C. Sims, S. R. Hunt, B. L. Corso, I. Perez, G. A. Weiss and P. G. Collins, *Science*, 2012, **335**, 319.
35 Y. Choi, T. J. Olsen, P. C. Sims, I. S. Moody, B. L. Corso, M. N. Dang, G. A. Weiss and P. G. Collins, *Nano Lett.*, 2013, **13**, 625.
36 P. C. Sims, I. S. Moody, Y. Choi, C. J. Dong, M. Iftikhar, B. L. Corso, Q. T. Gul, P. G. Collins and G. A. Weiss, *J. Am. Chem. Soc.*, 2013, **135**, 7861.
37 S. Sorgenfrei, C. Y. Chiu, R. L. Gonzalez, Y. J. Yu, P. Kim, C. Nuckolls and K. L. Shepard, *Nat. Nanotechnol.*, 2011, **6**, 125.
38 S. Sorgenfrei, C. Y. Chiu, M. Johnston, C. Nuckolls and K. L. Shepard, *Nano Lett.*, 2011, **11**, 3739.
39 F. Patolsky, G. F. Zheng, O. Hayden, M. Lakadamyali, X. W. Zhuang and C. M. Lieber, *Proc. Natl. Acad. Sci. U. S. A.*, 2004, **101**, 14017.
40 G. F. Zheng, F. Patolsky, Y. Cui, W. U. Wayne and C. M. Lieber, *Nat. Biotechnol.*, 2005, **23**, 1294.
41 E. Stern, J. F. Klemic, D. A. Routenberg, P. N. Wyrembak, D. B. Turner-Evans, A. D. Hamilton, D. A. LaVan, T. M. Fahmy and M. A. Reed, *Nature*, 2007, **445**, 519.
42 J. Wang, F. Shen, Z. Wang, G. He, J. Qin, N. Cheng, M. Yao, L. Li and X. Guo, *Angew. Chem., Int. Ed.*, 2014, **53**, 5038.
43 H. Bayley and P. S. Cremer, *Nature*, 2001, **413**, 226.
44 L. Soleymani, Z. C. Fang, E. H. Sargent and S. O. Kelley, *Nat. Nanotechnol.*, 2009, **4**, 844.
45 X. Guo, A. A. Gorodetsky, J. Hone, J. K. Barton and C. Nuckolls, *Nat. Nanotechnol.*, 2008, **3**, 163.
46 X. Guo, A. Whalley, J. E. Klare, L. M. Huang, S. O'Brien, M. Steigerwald and C. Nuckolls, *Nano Lett.*, 2007, **7**, 1119.
47 S. Liu, X. Y. Zhang, W. X. Luo, Z. X. Wang, X. Guo, M. L. Steigerwald and X. H. Fang, *Angew. Chem., Int. Ed.*, 2011, **50**, 2496.
48 H. F. Wang, N. B. Muren, D. Ordinario, A. A. Gorodetsky, J. K. Barton and C. Nuckolls, *Chem. Sci.*, 2012, **3**, 62.
49 S. Roy, H. Vedala, A. D. Roy, D. H. Kim, M. Doud, K. Mathee, H. K. Shin, N. Shimamoto, V. Prasad and W. B. Choi, *Nano Lett.*, 2008, **8**, 26.
50 H. T. Liu, J. He, J. Y. Tang, H. Liu, P. Pang, D. Cao, P. Krstic, S. Joseph, S. Lindsay and C. Nuckolls, *Science*, 2010, **327**, 64.
51 X. C. Qin, Q. Z. Yuan, Y. P. Zhao, S. B. Xie and Z. F. Liu, *Nano Lett.*, 2011, **11**, 2173.
52 X. Guo, J. P. Small, J. E. Klare, Y. L. Wang, M. S. Purewal, I. W. Tam, B. H. Hong, R. Caldwell, L. M. Huang, S. O'Brien, J. M. Yan, R. Breslow, S. J. Wind, J. Hone, P. Kim and C. Nuckolls, *Science*, 2006, **311**, 356.
53 Y. Cao, S. Dong, S. Liu, L. He, L. Gan, X. Yu, M. L. Steigerwald, X. Wu, Z. Liu and X. Guo, *Angew. Chem., Int. Ed.*, 2012, **51**, 12228.
54 C. Jia and X. Guo, *Chem. Soc. Rev.*, 2013, **42**, 5642.
55 L. Sun, Y. A. Diaz-Fernandez, T. A. Gschneidtner, F. Westerlund, S. Lara-Avilab and K. Moth-Poulsen, *Chem. Soc. Rev.*, 2014, **43**, 7378.
56 X. Guo, *Adv. Mater.*, 2013, **25**, 3397.
57 We define the cutting yield as the fraction of graphene transistors on a chip, which are electrically disconnected after oxygen plasma etching and the connection yield as the fraction of the completely-broken devices that get reconnected after molecular connection, respectively.
58 E. Ostuni, R. G. Chapman, R. E. Holmlin, S. Takayama and G. M. Whitesides, *Langmuir*, 2001, **17**, 5605.
59 M. Shim, N. Kam, R. Chen, Y. Li and H. Dai, *Nano Lett.*, 2002, **2**, 285.
60 I. C. Gherghi, S. T. Girousi, A. Voulgaropoulos and R. Tzimou-Tsitouridou, *Anal. Chim. Acta*, 2004, **505**, 135.
61 I. C. Gherghi, S. T. Girousi, A. N. Voulgaropoulos and R. Tzimou-Tsitouridou, *Talanta*, 2003, **61**, 103.
62 M. D. Baaske, M. R. Foreman and F. Vollmer, *Nat. Nanotechnol.*, 2014, **9**, 933.

